Complex-transfer-function analysis of optical-frequency converters

Derek Chang,[1,2,*] Carsten Langrock,[1] Yu-Wei Lin,[1] C. R. Phillips,[1,3] C. V. Bennett,[2] and M. M. Fejer[1]

[1]*E. L. Ginzton Laboratory, Stanford University, Stanford, California 94305, USA*

[2]*Lawrence Livermore National Laboratory, Livermore, California 94551, USA*

[3]*Department of Physics, Institute of Quantum Electronics, ETH Zurich, Zurich 8093, Switzerland*

**Corresponding author: djychang@stanford.edu*

Received June 26, 2014; accepted July 24, 2014;
posted July 28, 2014 (Doc. ID 214536); published August 22, 2014

The measurement of the magnitude and phase of the complex transfer function (CTF) of aperiodically poled lithium niobate waveguide devices using frequency resolved optical gating (FROG) is demonstrated. We investigate the sources of CTF distortions which are related to variations in the spatial distribution of the nonlinear coefficient and phase-mismatch profile and present a method to infer fabrication errors from the CTF discussed.

OCIS codes: (190.4360) Nonlinear optics, devices; (190.7110) Ultrafast nonlinear optics.
http://dx.doi.org/10.1364/OL.39.005106

Quasi-phase-matching (QPM) gratings can be used to tailor the frequency response of wavelength converters, a degree of freedom particularly useful for optical signal processing devices. In Ref. [1], the phase response was engineered to compensate for group-velocity mismatch and a transfer function formalism for second harmonic generation (SHG) was derived. The transfer function here represents the magnitude and phase of the output spectrum of a nonlinear mixing process compared to the inputs. This transfer function is independent of the input waves and only depends on intrinsic material properties and QPM design. This concept is useful for designing devices as well as analyzing the performance of QPM-based optical-frequency converters (OFC).

Transfer functions may exhibit distortions because of material defects or fabrication errors. In waveguide-based OFCs, longitudinally varying phase velocity inhomogeneities can arise from longitudinal variations in the waveguide lithography or processing conditions. In devices with a uniform, periodic grating, such inhomogeneities reduce the peak conversion efficiency and distort the ideal sinc^2 transfer function [2,3]. In chirped (aperiodic) gratings, each frequency component of the input converts at distinct positions along the propagation direction, and perturbations create uneven conversion efficiencies and therefore distort the passband of the transfer function. In practical devices, the QPM waveguide parameters are often designed to minimize the sensitivity of the phase-matching to fabrication errors; if the first-order dependence of the phase-mismatch with respect to a particular fabrication parameter, e.g., waveguide width, vanishes, the design is said to be noncritical [4], in relation to noncritical phase-matching in bulk frequency converters. However, large fabrication errors, or deviations of the design from the noncritical condition, may still introduce unwanted distortions to the transfer function, degrading device performance beyond acceptable limits.

While the transfer function can be measured by tuning a CW input laser across the bandwidth of the device and monitoring the amplitude and phase of the generated output [5], measuring the phase response by this approach is experimentally difficult. In this Letter, we introduce and experimentally demonstrate a method for measuring the CTF by characterizing the complex input and output spectra of ultrafast pulses, as well as the extraction of the spatial dependence of the effective nonlinear coefficient $d(z)$ and the phase mismatch $\Delta\beta(z)$. These functions, in turn, are useful for diagnosing fabrication defects, as well as for predicting the performance of the device in various phase-sensitive applications. We focus here on the SHG process, though the concepts can be extended straightforwardly to other mixing processes [6].

The CTF, $\hat{D}(\Omega) \equiv \hat{A}_2(\Omega)/\hat{A}_1^2(\Omega)$, for SHG, in the low conversion regime, is the ratio of the spectrum of output second harmonic (SH), $\hat{A}_2(\Omega)$, to the spectrum of the square of the input fundamental harmonic (FH) $\hat{A}_1^2(\Omega)$ here $\Omega = \omega - \omega_2$ is the frequency detuning from the SH carrier ω_2 and the hat notation denotes a Fourier transform such that $\hat{f}(\Omega)$ is the Fourier transform of $f(t)$. Assuming an undepleted pump and negligible group velocity dispersion (GVD) over the bandwidth of the pulse, the CTF is related to the nonlinear coefficient $d(z)$ by the following integral [7]:

$$\hat{D}(\Omega) = \int_{-\infty}^{\infty} \mathrm{d}(z) \exp\left[-\frac{1}{2}(2\alpha_1 - \alpha_2)z\right] \exp[i\Delta\phi(\Omega, z)]\mathrm{d}z, \quad (1)$$

where $\Delta\phi(\Omega, z) = \int_{-\infty}^{z} \Delta\beta(\Omega, z')\mathrm{d}z'$ is the phase mismatch, $\Delta\beta$ is the wave-vector mismatch, and $d(z)$ is the nonlinear coefficient. We assume $\hat{A}_2(\Omega, z = 0) = 0$ and that $d(z) = 0$ outside of the range $[0, L]$, where L is the length of the QPM grating. This form expands on that of Ref. [7] by including propagation power loss α_1 at the FH and α_2 at the SH. In the general case, we consider an apodized [8], nonuniform QPM grating whose apodization profile and variations in the local grating period and duty cycle are slow compared with the grating period itself, such that $d(z)$ can be accurately represented as a sum of distinct Fourier components $d_m(z)$, with a z-dependent amplitude and k-vector. We also assume that the mth component of the grating is phase-matched and dominates all other orders of the grating. In this case, the general form of $d(z)$ becomes

$$d(z) = d_m(z) = |d_m(z)| \exp[iK_{0m}z + i\Phi_m(z)], \quad (2)$$

where $|d_m(z)|$ is the amplitude of the mth Fourier component of the grating and $\Phi_m(z)$ represents the phase of the grating beyond the $K_{0m}z$ carrier phase.

Material and waveguide dispersion are represented by $\Delta\beta(\Omega, z)$. To introduce the functional dependence of $\Delta\beta$ on the spatial coordinate z, we introduce a parametric representation $\xi(z)$ such that $\Delta\beta(\Omega, z) = \Delta\beta(\Omega, \xi(z))$. If we assume the typical variation $\delta\xi$ in the parameter, e.g., the waveguide width, is small compared to the nominal parameter value ξ, we can perform a Taylor series expansion resulting in

$$\begin{aligned}\Delta\beta(\Omega, \xi(z)) = \Delta\beta_0 &+ \frac{\partial\Delta\beta}{\partial\Omega}\Omega + \frac{\partial\Delta\beta}{\partial\xi}\delta\xi + \frac{1}{2}\frac{\partial^2\Delta\beta}{\partial\Omega^2}\Omega^2 \\ &+ \frac{1}{2}\frac{\partial^2\Delta\beta}{\partial\xi^2}\delta\xi^2 + \frac{\partial^2\Delta\beta}{\partial\Omega\partial\xi}\Omega\delta\xi \\ &+ \frac{1}{2}\frac{\partial^3\Delta\beta}{\partial\Omega\partial\xi^2}\Omega\delta\xi^2 + \cdots, \end{aligned} \quad (3)$$

where $\Delta\beta_0 = \Delta\beta(0, 0)$ and all derivatives are evaluated at $\Omega = 0, \xi = 0$. We consider situations where only terms up to second order are significant. For the reverse proton-exchange waveguides considered here, the following inequality holds:

$$\frac{\partial\Delta\beta}{\partial\xi}\delta\xi + \frac{\partial^2\Delta\beta}{\partial\xi^2}\delta\xi^2 \gg \frac{\partial}{\partial\Omega}\left(\frac{\partial\Delta\beta}{\partial\xi}\delta\xi + \frac{\partial^2\Delta\beta}{\partial\xi^2}\delta\xi^2\right)\Omega_b. \quad (4)$$

This inequality shows that the first and second-order variations of $\Delta\beta$ with respect to the parameter ξ have negligible dependence on frequency over the bandwidth of the SH, Ω_b. As a result, $\Delta\beta$ is additively separable up to second-order and hence can be written as

$$\Delta\beta(\Omega, \xi(z)) = \Delta\beta_0 + \Delta\beta_\Omega(\Omega) + \Delta\beta_\xi(\xi(z)), \quad (5)$$

where

$$\begin{aligned}\Delta\beta_\Omega(\Omega) &= \frac{\partial\Delta\beta}{\partial\Omega}\Omega + \frac{1}{2}\frac{\partial^2\Delta\beta}{\partial\Omega^2}\Omega^2 \\ \Delta\beta_\xi(\xi) &= \frac{\partial\Delta\beta}{\partial\xi}\delta\xi + \frac{1}{2}\frac{\partial^2\Delta\beta}{\partial\xi^2}\delta\xi^2. \end{aligned} \quad (6)$$

If the device is designed to be noncritical for the parameter ξ, then phase-matching does not have a first-order dependence in ξ [3], i.e., $(\partial\Delta\beta/\partial\xi)\delta\xi = 0$.

Here, we introduce the notation $\hat{D}(\Omega) \equiv \hat{d}(\Delta k(\Omega))$ and the transfer function can be written as

$$\begin{aligned}\hat{d}(\Delta k_m) = \int_{-\infty}^{\infty} &|d_m(z)| \exp\left[-\frac{1}{2}(2\alpha_1 - \alpha_2)z\right] \\ &\times \exp[i\phi_m(z)] \exp[i\Delta k_m z]\mathrm{d}z, \end{aligned} \quad (7)$$

where

$$\Delta k_m(\Omega) = \Delta\beta_0 - K_{0m} + \Delta\beta_\Omega(\Omega), \quad (8)$$

$$\phi_m(z) = \Phi_m(z) + \int_0^z \Delta\beta_\xi(\xi(z'))\mathrm{d}z'. \quad (9)$$

The transfer function has a Fourier transform relationship with the product of the nonlinear coefficient and propagation loss factor. It follows that $|d_m(z)|$ and $\Delta\beta(\xi(z))$ can be derived directly from the transfer function:

$$|d_m(z)| = \exp\left[\frac{1}{2}(2\alpha_1 - \alpha_2)z\right] \cdot |\mathcal{F}^{-1}[\hat{d}(\Delta k_m)]|, \quad (10)$$

$$\Delta\beta_\xi(\xi(z)) = \frac{d}{dz}(\mathrm{Arg}\{\mathcal{F}^{-1}[\hat{d}(\Delta k_m)]\} - \Phi_m(z)), \quad (11)$$

where $\mathcal{F}^{-1}$ denotes the inverse Fourier transform. Deriving $|d_m(z)|$; and $\Delta\beta_\xi(\xi(z))$ from the transfer function $\hat{D}(\Omega)$ gives useful information about deviations of the device from its design values, because of issues such as fabrication errors and photorefractive effects. Deviations of $|d_m(z)|$; from ideal could result from duty cycle variations or QPM domain dropouts. Variations in $\Delta\beta_\xi(\xi(z))$ result from variations in waveguide dispersion which distort phase-matching.

The devices under test are aperiodically poled lithium niobate (A-PPLN) waveguides. The linearly chirped QPM gratings are 43 mm long and phasematch a bandwidth of 22 nm with a center wavelength of 1560 nm. Waveguides are formed by proton exchange (PE) in benzoic acid through a lithographically defined mask. The exchange depth is determined by the exchange time and temperature [9]. This step is followed by annealing and reverse-proton-exchange (RPE) steps which decrease propagation loss while increasing the modal overlap between interacting fields [10–12].

In our experimental setup, a Ti:sapphire-pumped optical parametric oscillator that outputs 150 fs duration transform-limited pulses at 80 MHz with an average power of 200 mW is used as the pump source (Opal, Spectra-Physics). The magnitude and phase of the pump are characterized by SHG Frequency Resolved Optical Gating (FROG) [13]. This FH pump has a full width half-maximum bandwidth exceeding the bandwidth of the QPM grating to ensure that the entire transfer function is sufficiently sampled. The SH pulse out of the PPLN waveguide device is characterized by a sum-frequency generation cross-FROG (SFG XFROG), where a fraction of the pump pulse is mixed with the SH pulse via noncollinear, type-I phase-matching in a 250 μm thick BBO crystal cut at an angle of 22.4°. The spectrum of the generated output of the BBO crystal is measured by a spectrometer (HR4000, Ocean Optics) centered at 520 nm. FROG software (FROG Scan 8, Mesaphotonics) was used to automate the measurement and retrieve the FROG trace.

We obtain low SHG (64×64 grid) and SFG (256×256 grid) FROG errors, 0.002 and 0.006, respectively. The spectra of the retrieved FH and SH are compared with independent measurements using an optical spectrum analyzer (Yokogawa AQ6370C), confirming measurement accuracy.

Once the input FH and output SH are measured, the CTF is calculated by dividing the spectrum of the SH by the spectrum of the square of the FH. Figure 1 shows the magnitude and phase of the measured CTF. Theoretically, the curvature of the phase is proportional to the chirp rate of the QPM grating, $D_g = \delta k/(2L)$, the ratio

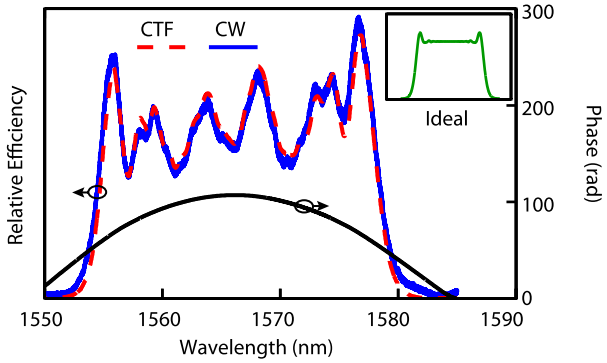

Fig. 1. Complex transfer magnitude (dashed, red) compared with CW magnitude (thick, blue) and ideal magnitude (inset). The phase (gray) curvature matches the theory to within 1%.

of the k-vector bandwidth δk of the linearly chirped QPM grating to the length of the QPM grating L [7]; the experimentally observed curvature agrees to within 1% with the predicted phase curvature based on the grating design. The magnitude of the transfer function was also measured with a tunable, continuous-wave (CW) laser at the FH wavelength. The ratio of the FH and SH power, $\sqrt{P_{\mathrm{SH}}/P_{\mathrm{FH}}^2}$, represents the magnitude of the transfer function. As can be seen from Fig. 1, the two independent measurements show good agreement. Slight discrepancies come from small errors in the FROG measurement, which can be further minimized by incorporating frequency marginals [14]; our FROG software did not have this capability. For comparison, the inset represents the designed magnitude transfer function. The sample shown here exhibits significant deviations from the ideal transfer function; the best devices we have fabricated show ~5% deviation from a flat passband.

Insight into the cause for these distortions is found by extracting $|d_m(z)|$; and $\Delta\beta(z)$ using Eqs. 10 and 11. The loss coefficients α_1 and α_2 were previously measured and correspond to 0.2 dB/cm at the FH and 0.1 dB/cm at the SH. Errors in the loss measurement will add an artificial slope to $|d_m(z)|$;. The grating phase is $\Phi(z) = D_g z^2$.

The measured nonlinear coefficient profile, $|d_m(z)|$;, shown in Fig. 2, is plotted together with the as-designed profile. It is nearly constant for the majority of the device and apodized near the edges at $z = 0$ and $z = L$ to prevent high-frequency ripples in the transfer function [8]. The measured apodization profile and length closely follows the design. The measured phase-mismatch error, $\Delta\beta_\xi(\xi(z))$, ideally zero for all z, clearly exhibits distortions. It can vary by as much as 500 m^{-1} over a length of about 10 mm. These ripples in $\Delta\beta_\xi(\xi(z))$ are the dominant cause of transfer function distortions.

The phase-mismatch errors can be attributed to four possible causes in our fabrication process: variations in the lithographically defined waveguide width, longitudinal variations in PE temperature, anneal furnace temperature, or RPE temperature. The effect of these variations is estimated by using a 2D diffusion model to map variations in these parameters to changes in the guided-mode effective indices, and hence to phase-mismatch errors. The variations in observed phase-mismatch errors correspond to either a 0.2 μm variation in the wet-etched SiO_2 mask, a 0.3°C variation in the PE bath temperature, a 2°C variation in the anneal furnace temperature, a 0.2°C variation in the RPE bath temperature, or a combination thereof. The corresponding waveguide-mask width error is illustrated in Fig. 2. To test the uniformity of the waveguide width, we measured the mask openings of two waveguides on a chip fabricated under identical conditions to the chip mentioned above. Using an atomic force microscope (AFM), the chip is sampled 32 times every 2 mm in the longitudinal direction. The standard deviation of widths of each waveguide over the 32 scans has an average value of 0.04 μm with a median value that varies about 0.2 μm over the length of the device, which is consistent with the CTF calculation. This waveguide width error appears to be the dominant effect and explains the majority of the $\Delta\beta$ error. If these errors can be reduced significantly, investigation of and possible improvements to the temperature uniformity of the exchange processes should be performed.

The CTF of 12 waveguides, spaced 400 μm apart, are measured and the resulting $\Delta\beta_\xi(\xi(z))$ profiles are shown in Fig. 3. There are bright bands at $z = 17$ mm and $z = 31$ mm signifying a strong correlation across the entire device, which strongly suggests that the phase-matching error of each waveguide is caused by global fabrication problems.

There are a few things to note about this technique. The calculated $|d_m(z)|$; is not in absolute units. A

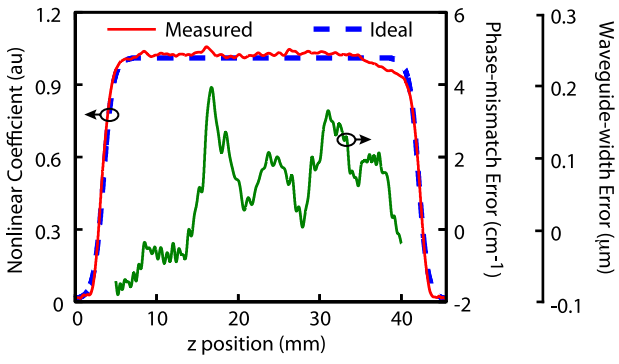

Fig. 2. Nonlinear coefficient $|d_m(z)|$; measured (solid) and as-designed (dash). Phase-mismatch error $\Delta\beta_\xi(\xi(z))$ and corresponding waveguide-mask width error.

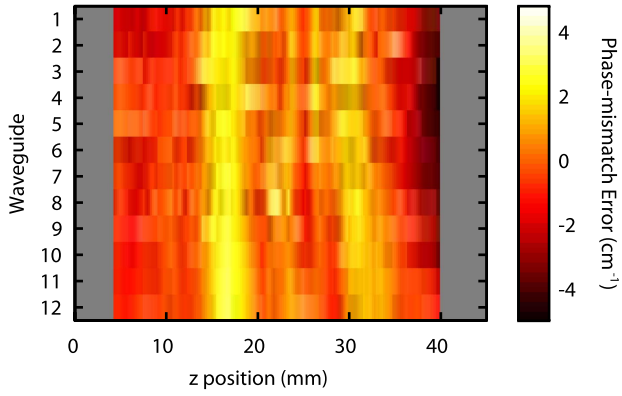

Fig. 3. Phase-mismatch error of 12 equidistantly spaced waveguides with a total separation of 4.4 mm.

separate measurement is needed for absolute scaling. The phase-mismatch, however, is in absolute units. Additionally, we neglect GVD and higher order dispersion at the FH. In our case, the effect of GVD is small as it contributes 0.1 rad of spectral phase over the bandwidth and length of the device. Neglecting GVD leads to a convenient one-to-one mapping between optical frequency of the generated wave and spatial frequencies of the QPM grating structure; this property is used to construct the CTF. In cases where the FH accumulates non-negligible group delay dispersion (GDD) over the length of the device, there is a finite spread of QPM grating spatial frequencies that can generate a particular SH optical frequency. To account for FH-GDD, a more general analysis discussed in [15] can be performed. In this analysis, the transfer function used here is replaced with a transfer matrix that describes the general mapping between grating spatial frequency and generated optical frequency including all orders of dispersion at both waves. Finally, the spatial resolution δz is limited by the resolvable frequency content of the CTF. If the CTF passband is resolved, then the bandwidth δk determines δz. For a chirped grating, δk is determined by the length L and chirp rate D_g of the QPM grating. Assuming the CTF to be a perfect top hat, the point spread function would have a sinc profile and the resolvable distance is $\delta z = 2\pi/\delta k = \pi/D_g L$. The device used in this study has a chirp rate of $D_g = 0.14\ \text{mm}^{-2}$ and a grating length of $L = 43$ mm, resulting in $\delta z = 0.5$ mm. However, in our measurement, we are able to resolve a spectral range of twice the CTF bandwidth, giving us a resolution of $\delta z = 0.25$ mm.

In conclusion, we have described and implemented a method for measuring the CTFs of QPM nonlinear devices and relating these CTFs to spatial variations in fabrication parameters. Further discussion of these errors and their implications for the performance of time lensing systems will be given in a subsequent paper.

The authors thank Dan Kane for his helpful advice and support. This work performed under the auspices of U.S. Department of Energy by LLNL under contract (DE-AC52-07NA27344). In addition, we gratefully acknowledge the support of the Lawrence Scholar Program and AFOSR (FA9550-12-1-0110).

References

1. M. A. Arbore, O. Marco, and M. M. Fejer, Opt. Lett. **22**, 865 (1997).
2. S. Helmfrid, G. Arvidsson, and J. Webjorn, J. Opt. Soc. Am. B **10**, 222 (1993).
3. M. L. Bortz, S. J. Field, M. M. Fejer, D. W. Nam, R. G. Waarts, and D. F. Welch, IEEE J. Quantum Electron. **30**, 2953 (1994).
4. E. J. Lim, S. Matsumoto, and M. M. Fejer, Appl. Phys. Lett. **57**, 2294 (1990).
5. R. Schiek, Y. Baek, and G. I. Stegeman, J. Opt. Soc. Am. B **15**, 2255 (1998).
6. G. Imeshev, M. M. Fejer, A. Galvanauskas, and D. Harter, J. Opt. Soc. Am. B **18**, 534 (2001).
7. G. Imeshev, M. A. Arbore, and M. M. Fejer, J. Opt. Soc. Am. B **17**, 304 (2000).
8. J. Huang, X. P. Xie, C. Langrock, R. V. Roussev, D. S. Hum, and M. M. Fejer, Opt. Lett. **31**, 604 (2006).
9. R. W. Boyd, *Nonlinear Optics* (Academic, 2008).
10. Y. N. Korkishko, V. A. Fedorov, T. M. Morozova, F. Caccavale, F. Gonella, and F. Segato, J. Opt. Soc. Am. A **15**, 1838 (1998).
11. J. Olivares and J. M. Cabrera, Appl. Phys. Lett. **62**, 2468 (1993).
12. R. Roussev, A. Sridharan, K. Urbanek, R. Byer, and M. M. Fejer, in *IEEE LEOS Annual Meeting Conference* (IEEE, 2003), pp. 334–335.
13. R. Trebino, K. W. Delong, D. N. Fittinghoff, J. N. Sweetser, B. A. Richman, M. A. Krumbu, and D. J. Kane, Rev. Sci. Instrum. **68**, 3277 (1997).
14. K. W. DeLong, D. N. Fittinghoff, and R. Trebino, IEEE J. Quantum Electron. **32**, 1253 (1996).
15. C. R. Phillips, L. Gallmann, and M. M. Fejer, Opt. Lett. **21**, 843 (2013).